A DFT+U study of the structural, electronic, magnetic, and mechanical properties of cubic and orthorhombic $SmCoO_3$

Cite as: J. Chem. Phys. **145**, 224704 (2016); https://doi.org/10.1063/1.4971186
Submitted: 30 September 2016 . Accepted: 17 November 2016 . Published Online: 08 December 2016

Emilia Olsson, Xavier Aparicio-Anglès, and Nora H. de Leeuw

A DFT+U study of the structural, electronic, magnetic, and mechanical properties of cubic and orthorhombic $SmCoO_3$

Emilia Olsson,[1] Xavier Aparicio-Anglès,[1] and Nora H. de Leeuw[1,2,a)]
[1]*Department of Chemistry, University College London, WC1H 0AJ London, United Kingdom*
[2]*School of Chemistry, Cardiff University, Main Building, Park Place, CF10 3AT Cardiff, United Kingdom*

(Received 30 September 2016; accepted 17 November 2016; published online 8 December 2016)

$SmCoO_3$ is a perovskite material that has gained attention as a potential substitute for $La_{1-x}Sr_xMnO_{3-d}$ as a solid oxide fuel cell cathode. However, a number of properties have remained unknown due to the complexity of the material. For example, we know from experimental evidence that this perovskite exists in two different crystal structures, cubic and orthorhombic, and that the cobalt ion changes its spin state at high temperatures, leading to a semiconductor-to-metal transition. However, little is known about the precise magnetic structure that causes the metallic behavior or the spin state of the Co centers at high temperature. Here, we therefore present a systematic DFT+U study of the magnetic properties of $SmCoO_3$ in order to determine what magnetic ordering is the one exhibited by the metallic phase at different temperatures. Similarly, mechanical properties are difficult to measure experimentally, which is why there is a lack of data for the two different phases of $SmCoO_3$. Taking advantage of our DFT calculations, we have determined the mechanical properties from our calculated elastic constants, finding that both polymorphs exhibit similar ductility and brittleness, but that the cubic structure is harder than the orthorhombic phase. [http://dx.doi.org/10.1063/1.4971186]

I. INTRODUCTION

Solid oxide fuel cells (SOFC) are considered potential alternatives to today's power generators. In order to expand the applicability of these devices, their reliability and cost need to be improved, goals which can be achieved by lowering the operating temperatures.[1,2] However, this has proven to be challenging, since the efficiency of traditional SOFC is compromised when the operating temperatures are lowered. Some of the problems that have been encountered are cathodic polarization, increase in the resistance in the cell, or reduced catalytic activity, among others.[3] Many of these issues relate to the cathode's performance, which is required to have high catalytic activity for the oxygen reduction reaction (ORR), and which should also facilitate oxygen conduction to the electrolyte.[3] To this end, cobalt-based perovskites have gained much attention as cathodic materials, especially $SmCoO_3$, since it shows high catalytic efficiency and good mixed conductivity at intermediate operating temperatures.[4–13] Interestingly, both theoretical and experimental data on $SmCoO_3$-based perovskites are rather scarce, including its magnetic and mechanical properties, because more research has focused on the related $LaCoO_3$ material.

$SmCoO_3$ is found in two different crystal structures; orthorhombic and cubic (Fig. 1). The orthorhombic structure is the most stable phase at low temperatures, whereas the cubic structure is stabilized when the material is doped and at high temperatures.[14] The temperature also influences the electronic and magnetic properties of $SmCoO_3$. The electronic behavior has been studied experimentally, and a semiconductor to metal transition has been reported at temperatures higher than 500 K.[15–17] This transition is suggested to be due to a change in the cobalt spin state.[15–19] At the same time, the Co spin state is heavily influenced by the local structure, dopant substitution, and applied external pressure, and it is normal to find different spin domains or the coexistence of two spin states in the same sample.[19] To add further complexity, the spin consequently affects the magnetic structure and vice versa,[19] which at the same time will influence the chemistry of $SmCoO_3$. Thus, there is a clear interest in understanding which spin state is coupled to a certain magnetic structure and which magnetic structure is the most likely to be responsible for the metallic state observed at high temperatures.

Mechanical stability of SOFC cathodes is also of importance for the performance and stability of the fuel cell, especially for industrial scalability, a fact that is often overlooked in fundamental studies.[20] SOFC materials should have thermal compatibility with the electrolyte, good mechanical strength, and be tough.[1,21] It is further undesirable to have large mechanical deformation at operating temperatures, and an understanding of the mechanical properties such as bulk and Young's moduli is useful.[1,20,21] To the best of our knowledge, there are no reported experimental values for the mechanical properties or elastic constants of $SmCoO_3$, neither for the cubic nor the orthorhombic structure. For the determination of the elastic constants, large single crystals with very high

a)Author to whom correspondence should be addressed. Electronic mail: deleeuwn@cardiff.ac.uk

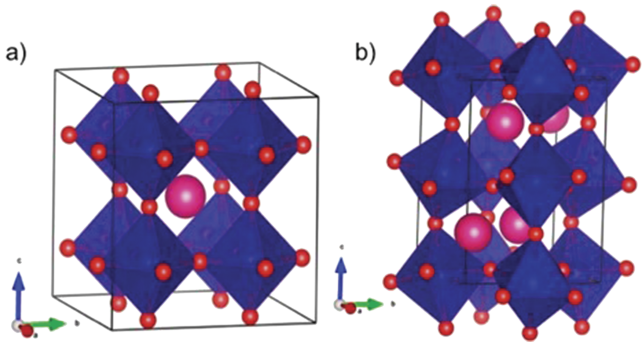

FIG. 1. Graphical polyhedral representation of (a) cubic and (b) orthorhombic $SmCoO_3$. Pink spheres are Sm, blue Co, and red O. Sm atoms are also placed in the center of the edges and faces, but are not shown here for clarity.

purity are required, and this is difficult to achieve for many perovskites.[22,23]

Thus, despite the availability of some experimental data on $SmCoO_3$, detailed information is lacking, including the antiferromagnetic arrangement and the Co spin state at high temperatures, or the precise values of the main mechanical properties. *Ab initio* calculations represent a powerful tool to provide insight into these properties and, in this paper we have used density functional theory (DFT) calculations to study the magnetic structure and the mechanical properties for the two polymorphs of $SmCoO_3$, taking into account the effect of temperature by simulating the thermal expansion of the material.

II. COMPUTATIONAL DETAILS

The Vienna *Ab initio* Simulation Package (VASP version 5.3.5) code has been used for all calculations.[24–27] We have used DFT to perform spin-polarized simulations with the PBE functional to describe the correlation-exchange interaction.[28,29] The project-augmented wave (PAW) method was used to describe the ion-electron interaction,[30] and we considered the following valence electrons for the atomic species involved: Sm ($5s^2 5p^6 6s^2$), Co ($4s^2 3d^7$), and O ($2s^2 2p^4$). Sm *f*-electrons were included in the pseudopotential as core electrons as the samarium ion in $SmCoO_3$ is +3 charged. The kinetic energy cut-off for the plane-wave basis set was set to 500 eV after testing it for both crystal structures. Structure optimizations were performed with the conjugate gradient method, considering electronic and ionic convergence criteria of 1×10^{-5} eV and 1×10^{-3} eV $Å^{-1}$, respectively. The tetrahedron method was used for the smearing,[31] and was applied together with a $4 \times 4 \times 4$ Γ-centered Monkhorst-Pack grid for the cubic model and $8 \times 8 \times 6$ for the orthorhombic model, to describe the reciprocal space.[32] The bulk models used throughout this paper are the $2 \times 2 \times 2$ *Pm*-3*m* cubic cell and the $2 \times 1 \times 1$ *Pnma* orthorhombic cell, both containing 40 atoms (Fig. 1). Finally, in order to properly describe the electronic and magnetic structures of $SmCoO_3$, the Hubbard approximation was employed as described in the Dudarev approximation.[33] Hence, we have applied a U_{eff} = 3 eV to the Co d-electrons, as done in our previous publications.[34]

III. RESULTS AND DISCUSSION

A. Structural properties

From the two reported crystal structures of $SmCoO_3$, the orthorhombic phase (*Pnma*) is known to be more stable than the cubic phase (*Pm*-3*m*) at low temperatures.[35–37] However, when $SmCoO_3$ is used for SOFC (normally doped and operating at high temperatures), the cubic phase becomes the more stable.[38,39] Our calculations indicate that, as observed experimentally, the orthorhombic phase is 0.13 eV $atom^{-1}$ lower in energy than the cubic phase. Both structures show good agreement with the experimental structural data, as shown in Table I, indicating that the Hubbard parameter used for the cubic phase is transferable to the orthorhombic system. The only noticeable difference with experiment is the lattice parameter *b* for the orthorhombic system, which is ~1.7% larger than the experimental value. This discrepancy has also been seen in previous theoretical work on orthorhombic cobalt perovskites.[40] This larger *b* parameter induces deviations in the bond lengths that are parallel to the *b* direction. Fortunately, the largest elongation for the Co–O bonds is only 0.03 Å, whereas the Sm–O bonds are stretched by a maximum of 0.14 Å.

B. Electronic and magnetic structures

The magnetic properties of lanthanide cobaltate perovskites are attributed to the Co^{3+} atoms.[17,18] Co^{3+} is a d^6 center, which is hexa-coordinated withO^{2-}anions in an

TABLE I. Calculated lattice parameters and Sm/Co–O bond lengths for the cubic and the orthorhombic $SmCoO_3$. Experimental data, when available, are included in brackets. Of the experimental data, the cubic structure has been obtained from Wold and Ward,[36] whereas orthorhombic experimental data were obtained from Perez-Cacho *et al.*[41] All values are expressed in Ångström.

Structure	a (Å)	b (Å)	c (Å)	Sm–O (Å)	Co–O (Å)
Cubic		3.75 (3.75)		2.65 (2.65)	1.88 (1.88)
Orthorhombic	5.29 (5.28)	5.44 (5.35)	7.53 (7.50)	2.30 (2.27)	1.94
				2.34 (2.35)	1.95
				2.37 (2.41)	1.96 (1.93)
				2.50 (2.53)	
				2.64 (2.61)	
				3.06 (3.05)	
				3.37 (3.23)	

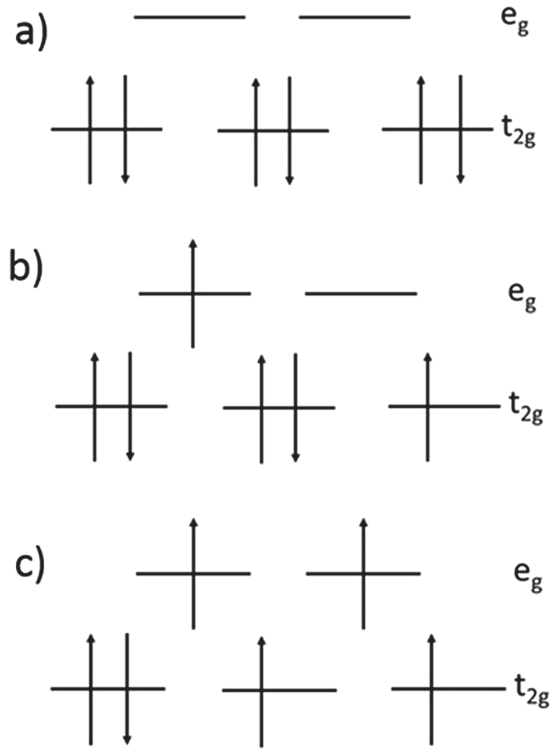

FIG. 2. Schematic representation of the three possible spin states for the Co d-orbital; (a) low, (b) intermediate, and (c) high spin state, assuming maximum multiplicity.

octahedral configuration in thecubic structure, and in a distorted octahedron in the orthorhombic structure. According to crystal field theory (CFT), the octahedral crystalfield splits the five d-orbitals between the t_{2g} (d_{xy}, d_{yz}, and d_{xz}) and the e_g (d_{x2-y2} and d_{z2}), withthe former being lower in energy than the latter. Depending on the occupancy of these orbitals, we distinguish between three different spin states for Co^{3+}: (a) low spin state (LS, $t_{2g}^6 e_g^0$) with S = 0; (b) intermediate spin state (IS, $t_{2g}^5 e_g^1$) with S = 1; and (c) high spin state (HS, $t_{2g}^4 e_g^2$) with S = 2, all of them schematically represented in Fig. 2.[15,16] We are assuming that the occupation of these orbitals will obey Hund's rule, i.e., that the most stable configurations should be those that maximize the spin multiplicity. For example, HS is S = 2 if and only if all unpaired electrons are either α or β.

TABLE II. Bader charges (q) and bandgap (E_g) in eV for both phases and all magnetic configurations for $SmCoO_3$.

	LS	AAFM	CAFM	GAFM	FM
q^{Sm}_{Cubic}	2.00	2.02	2.05	2.06	1.95
$q^{Sm}_{Orthorhombic}$	2.15	2.14	2.14	2.15	2.15
q^{Co}_{Cubic}	1.31	1.30	1.38	1.32	1.22
$q^{Co}_{Orthorhombic}$	1.44	1.61	1.61	1.45	1.47
q^{O}_{Cubic}	−1.10	−1.10	−1.14	−1.12	−1.06
$q^{O}_{Orthorhombic}$	−1.19	−1.27	−1.25	−1.20	−1.20
E_g^{Cubic} (eV)	0.68	0	0	0	0
$E_g^{Orthorhombic}$ (eV)	1.2	0	0	0.79	0.82 (β)

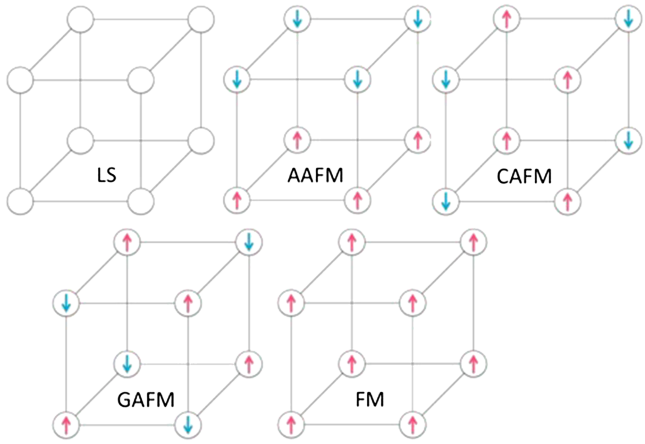

FIG. 3. Graphical representation of the different magnetic structures. For simplicity, each sphere represents a Co atom in the cubic phase, and this scheme is transferable to the orthorhombic phase. Pink up-arrows represent α alignment, whereas blue down-arrows represent β alignment, regardless of the spin state of the cobalt centers.

However, due to the nature of DFT, it becomes very complicated to determine pure intermediate or high spin states, and they normally appear as a combination. In the HS case, we can have three α electrons and one β, which means S = 1, or two α and two β, which describes a singlet state, which explains why in Table II, Co magnetization can be found between 0 and 4 μ_B, depending on the spin state.

For LS states, the system becomes diamagnetic. However, when Co^{3+} centers are found in IS or HS, we can distinguish four different paramagnetic structures, as shown in Fig. 3: three antiferromagnetic (AFM) structures, labeled AAFM, CAFM, and GAFM, and one ferromagnetic, labeled as FM.

Magnetic moments for samarium and oxygen ions are negligible in relation to their cobalt neighbors and they have consequently been omitted. The Bader charges (Table II) on Sm and O show negligible variance with magnetic moment and analysis also showed that the magnetic structure seems to have little to no impact on the charge of the different atoms in the material. Noticeably though, the orthorhombic phase shows higher charges throughout compared to the cubic phase, which could imply that the orthorhombic phase is more ionic than the cubic phase (Table II).

1. Diamagnetic structures

From the projected density of state (PDOS), we observe that for the $SmCoO_3$ diamagnetic (DM) cubic structure (Fig. 4(a)) the Co t_{2g} orbitals describe the valence band, in combination with the O 2p band, whereas the conduction band is defined by the Co e_g orbitals. The bandgap between the conduction and valence bands is 0.68 eV. This picture agrees completely with the crystal field theory prediction for the LS state of Co ions. However, the orthorhombic structure also gives rise to an insulator material, with a larger bandgap of 1.20 eV (Fig. 4(b)). In this case, however, the CFT cannot be used to describe the electronic structure as t_{2g} and e_g appear at the same energies, suggesting a distortion of the octahedral environment of the cobalt centers. Therefore, both valence and

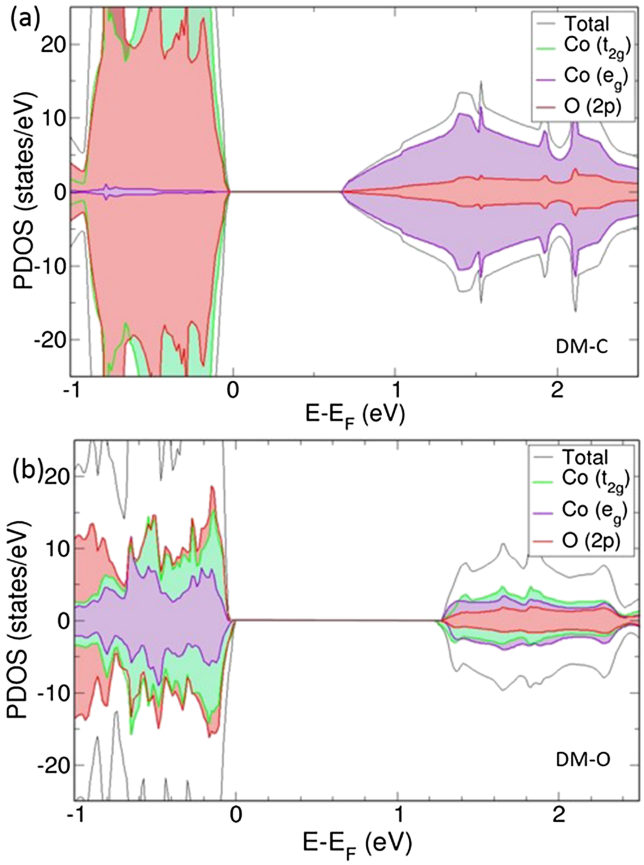

FIG. 4. PDOS for (a) cubic and (b) orthorhombic diamagnetic $SmCoO_3$.

conduction bands are described by a combination of t_{2g} and e_g orbitals, and the O 2p band. For the diamagnetic structures, both materials show $\mu_{Co} = 0\ \mu_B$.

2. Antiferromagnetic structures

In the AFM structures, the formal splitting of the Co^{3+} d-orbitals is not as clear as it was for the DM. One fact that is common for almost all structures regardless of the crystallographic phase is that $SmCoO_3$ becomes metallic, as there is no bandgap at the Fermi level (Fig. 5). This behavior has previously been observed in related perovskites.[40] Specifically, the orthorhombic phase becomes metallic when it has an A- or CAFM structure, but it remains a semiconductor when the material has a GAFM structure. This suggests that the experimentally observed insulator to metal transition would not involve the GAFM magnetic structure. Furthermore, since all three magnetic structures show non-split t_{2g}- and e_g-orbitals, electronic conduction goes through the d-metal band, without orbital preference.

Conversely, all cubic antiferromagnetic systems show metallic behavior. The electronic structures for AAFM and GAFM show that conduction is mainly through the t_{2g} Co orbitals, whereas for the CAFM it is mainly through the e_g, with a small contribution of the t_{2g}. Spin density plots for the calculated magnetic structure for the cubic and orthorhombic systems are included in Figures 6 and 7. Examining these, it can be seen that the spin ordering presented in Fig. 3 has been preserved in the calculations.

3. Ferromagnetic structure

Since the ferromagnetic structure has a non-zero total spin, α and β PDOS are not symmetric (Fig. 8). The cubic FM structure has metallic behavior, where the t_{2g} combined with the O 2p defines the β conduction and valence band, and e_g with the O 2p describes the α bands. For orthorhombic FM, a pure half-metallic structure was found, agreeing with previous experimental results found for other perovskites, such as FM $LaCoO_3$, where FM ordering has been assigned to an IS state.[40,42,43] Again, Co d-states are mixed t_{2g} and e_g, but the occupied states in spin-up direction at the Fermi level are mainly O 2p, with a Co d bandgap of 0.82 eV in the β spin.

4. Cobalt magnetic moments

The magnetic moments for the cobalt magnetization in the cubic structures are slightly lower compared to the orthorhombic phase (Table III). The differences in different magnetic structures between the phases are between 0.6 and 0.7 μ_B for AAFM and CAFM, and nearly 1.0 μ_B for FM. As a consequence, for AAFM, CAFM, and FM magnetic structures, the cubic phase presents Co centers in a mixed LS and IS state, but they are clear IS states for the orthorhombic phase.

The most remarkable difference is found for the GAFM structure. In both phases, Co magnetization is between 0.6 and 1 μ_B higher compared to the rest of the magnetic structures, and they are very similar for both polymorphs, 2.94 μ_B for the orthorhombic and 2.88 μ_B for the cubic phase. As a result, in the GAFM structure, Co spin states are mixed IS and HS.

5. Insulator-to-metal transition

To evaluate the evolution of the magnetic structure with temperature (Fig. 9), we have mimicked the volume expansion using the isotropic thermal expansion coefficient (α_T) for the orthorhombic $SmCoO_3$, $\alpha_T = 2.17 \times 10^{-5}\ K^{-1}$.[6] The linear thermal expansion coefficient is related to the lattice parameters, and thus supercell volume, through[44]

$$\alpha = \frac{1}{l_0}\frac{dl}{dT}, \tag{1}$$

where l is the lattice parameter, l_0 is the initial lattice parameter (here the reference is the ground state), and T is the temperature. The same thermal expansion coefficient was assumed for the cubic phase, since to the best of our knowledge no thermal expansion coefficient has been reported for this phase. In addition, we assumed that the thermal expansion was linear with respect to the temperature. For the calculations, the expanded volumes were kept fixed, whereas the ion positions were allowed to relax.

Examining Fig. 9, it can be seen that, as predicted experimentally, the diamagnetic structure is the ground state for both polymorphs, and the antiferromagnetic structures are higher in energy at low temperatures. At 500 K the CAFM and the DM states become nearly degenerated for the orthorhombic phase. However, due to the small relative energy differences, we believe that there would be coexistence of both states. These results are in line with the experimental transition found above 500 K.

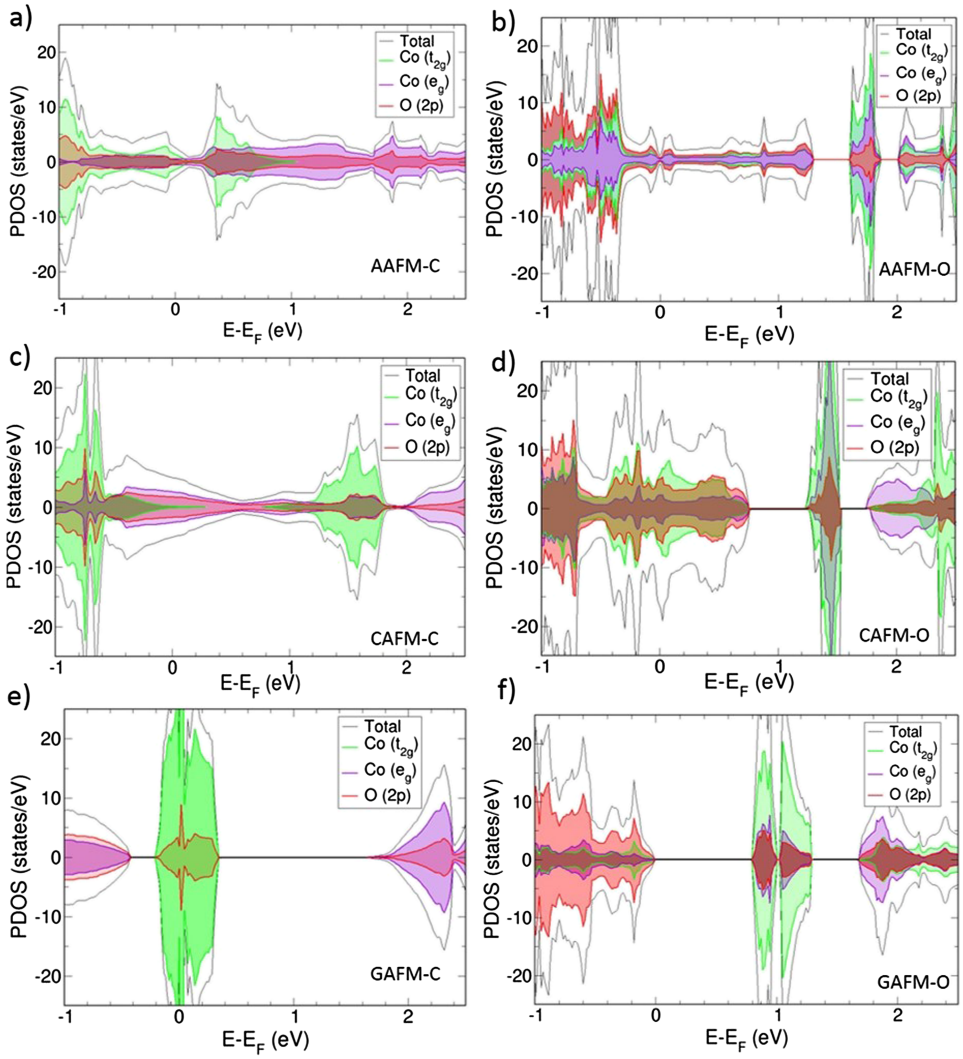

FIG. 5. PDOS for (a) cubic AAFM, (b) orthorhombic AAFM, (c) cubic CAFM, (d) orthorhombic CAFM, (e) cubic GAFM, and (f) orthorhombic GAFM.

For the cubic structure, however, we observe a clear crossing between the DM and the CAFM at around 1100 K in which the latter becomes almost 1 eV more stable than the former. This behavior is indeed in full agreement with the experimental results, which as previously noted, predicts an antiferromagnetic structure for the metallic state. It is important to highlight here that at these high temperatures the phase transition from orthorhombic to cubic is known to occur, and

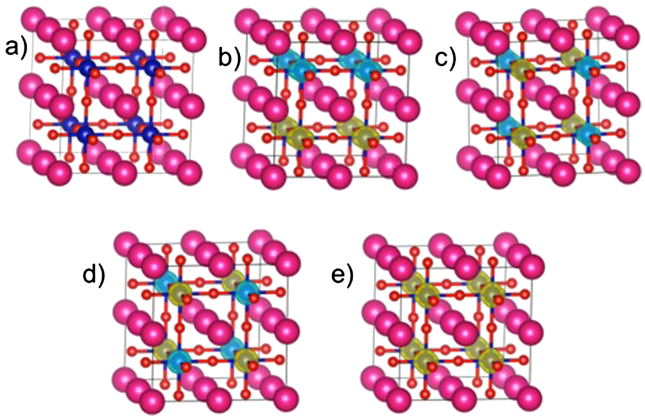

FIG. 6. Spin density plots of (a) diamagnetic, (b) AAFM, (c) CAFM, (d) GAFM, and (e) FM cubic magnetic structures. Pink spheres are samarium, blue cobalt, and red oxygen. Yellow spin density represents spin up, and light blue spin down. Surface iso-value is 0.05.

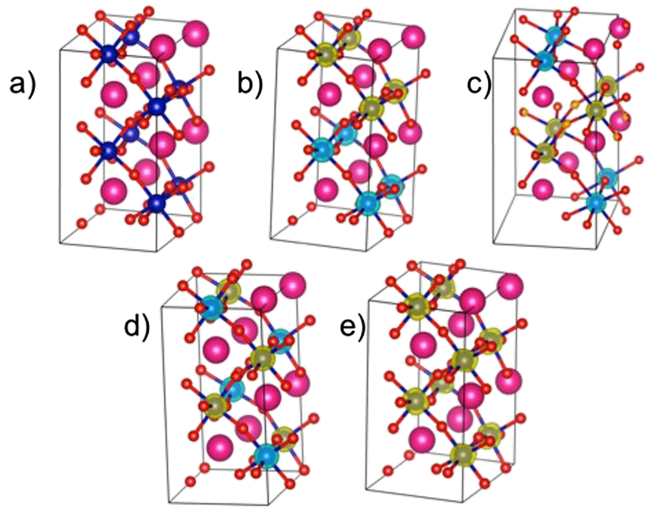

FIG. 7. Spin density plots of (a) diamagnetic, (b) AAFM, (c) CAFM, (d) GAFM, and (e) FM orthorhombic magnetic structures. Pink spheres are samarium, blue cobalt, and red oxygen. Yellow spin density represents spin up, and light blue spin down. Surface iso-value is 0.05.

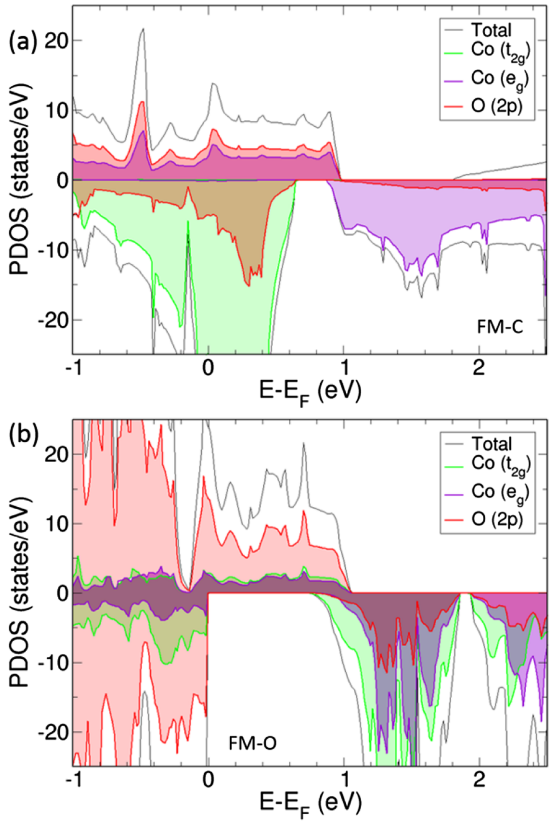

FIG. 8. PDOS for (a) cubic and (b) orthorhombic FM $SmCoO_3$.

according to our results, the insulator to metal transition is coupled with it.[14]

The stabilization of the CAFM structure seems to be related with the change in Co magnetic moment due to temperature. As depicted in Fig. 10, the magnetic moment of cobalt is initially 1.72 μ_B, and slightly increases with temperature until 1000 K. After that point, we can observe a drastic change in the Co magnetic moment, which reaches 2.93 μ_B at 1273 K. This increase is related to the deformation of the system, which is now pseudo-cubic, in agreement with a previous high temperature synthesis of $SmCoO_3$.[14]

C. Mechanical properties

Mechanical properties are obtained from the elastic constants (C_{ij}). C_{ij} were computed in VASP, using the finite difference technique to calculate the Hessian matrix. In the finite difference technique, displacements of each ion are made in the direction of each Cartesian coordinate in the lattice, with the Hessian being determined from the atomic displacements.

TABLE III. Cobalt magnetic moments (μ) in μ_B for cubic and orthorhombic $SmCoO_3$ in different magnetic structures.

	μ^{Co}_{Cubic} (μ_B)	$\mu^{Co}_{Orthorhombic}$ (μ_B)
DM	0.00	0.00
AAFM	1.28	2.01
CAFM	1.71	2.34
GAFM	2.88	2.94
FM	1.03	2.02

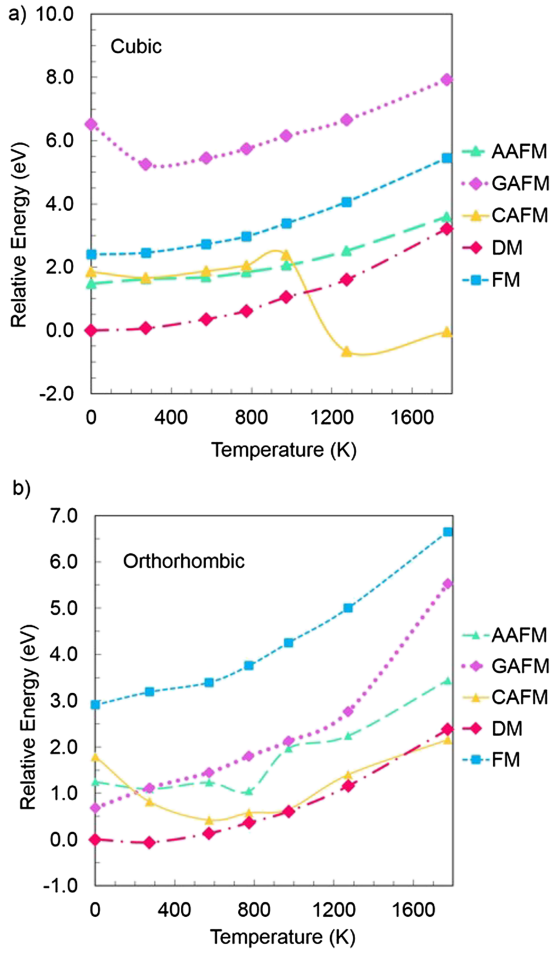

FIG. 9. Relative energies of magnetic structures with respect to DM (0 K) versus temperature for (a) cubic and (b) orthorhombic $SmCoO_3$. Please note that temperature is related to the supercell volume.

To reduce computational effort, only non-equivalent symmetry displacements are considered. The elastic tensor is then calculated by distorting the original lattice and derived using the strain-stress relationship, with the elastic constants calculated according to Eq. (2).[22,45,46] Due to symmetry operations, cubic materials have three independent elastic constants,[47] whereas orthorhombic systems have nine,[48]

$$C_{ij} = \frac{1}{V}\frac{\partial^2 E}{\partial\varepsilon_i \partial\varepsilon_j}. \quad (2)$$

The calculated C_{ij} can be found in Table IV. Generally speaking, C_{ii} relate to the material's response to a uniform pressure that is applied perpendicularly to each cell face. A distortion affecting two non-equal axes is represented by C_{ij} and its equivalents.[45,49] Also, specifically for cubic materials, the Cauchy relation ($C_{12} = C_{44}$) should hold,[45] although real materials do not always obey it.[50,51] For example, in our cubic $SmCoO_3$, this violation is observed since C_{12} = 75.89 GPa, and C_{44} = 100.72 GPa (Table IV). This is in disagreement with previously published molecular dynamics-derived data,[23] but it may be due to short-comings in the interatomic potential model, as the shell model is known to favor solutions that do not violate the Cauchy relation.[51,52]

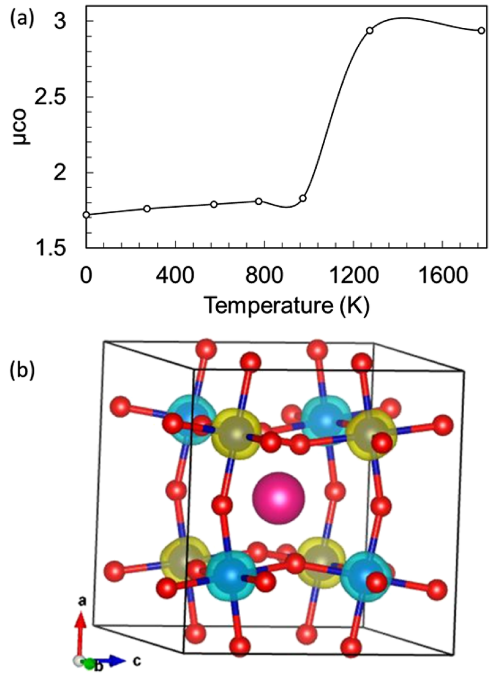

FIG. 10. (a) Cobalt magnetic moment in the cubic CAFM magnetic structure as a function of temperature (K). (b) Structure of the pseudo-cubic CAFM structure $SmCoO_3$ at 1273 K. Please note that the temperature is related to the supercell volume.

In addition, the elastic constants have to adhere to the general rules for mechanical stability. These relations differ depending on the symmetry of the crystal. In the case of cubic crystals, C_{ij} should accomplish:[45] $C_{11} - C_{12} > 0$, $C_{11} + 2C_{12} > 0$, and $C_{44} > 0$, whereas for orthorhombic crystals:[49] $C_{11} + C_{22} > 2C_{12}$, $C_{22} + C_{33} > 2C_{23}$, $C_{11} + C_{33} > 2C_{13}$, $C_{ii} > 0$, and $C_{11} + C_{22} + C_{33} + 2C_{12} + 2C_{13} + 2C_{23} > 0$. The elastic constants obtained here fulfill these conditions for both materials.

From the elastic constants, mechanical properties were calculated using Equations (3)–(13) which are collected in Table V.[53] Equations (3), (5), (7), and (10) are valid for cubic systems since C_{11}, C_{12}, and C_{44} are the complete set of independent elastic constants.[47] Orthorhombic crystals, on the other hand, have a larger set of independent elastic constants, and their mechanical properties are calculated using Equations (4), (6), (8), and (11)–(13).[49] For clarity, superscripts *c* and *o* are used to indicate the cubic and orthorhombic crystal, respectively. Furthermore, the bulk and shear moduli have been calculated using the Voigt approximation.[45,47,49,54]

TABLE IV. Elastic constants for $SmCoO_3$.

	Cubic	Orthorhombic
C_{11} (GPa)	461.60	244.84
C_{12} (GPa)	75.89	86.09
C_{44} (GPa)	100.72	99.82
C_{22} (GPa)		154.40
C_{33} (GPa)		300.65
C_{55} (GPa)		105.38
C_{66} (GPa)		85.62
C_{13} (GPa)		84.76
C_{23} (GPa)		49.21

1. Bulk modulus (B)

The bulk modulus (B) (Eqs. (3) and (4)) is the material's ability to resist a uniform compression (i.e., fracture resistance). It has been shown experimentally that for ABO_3 perovskites, B is dependent on the lattice volume, with larger cell volumes leading to smaller B through an inverse relationship.[45] Our calculated bulk moduli follow this behavior. B^O is 126.67 GPa, whereas B^C = 204.46 GPa, with the volume for the orthorhombic cell being larger than the cubic. Comparison with an experimental study made on $LaCoO_3$ at room temperature, whose orthorhombic bulk modulus is 122 GPa, shows that our results show a good match with general cobaltate perovskites.[55] The scale of B can also be related to the material's hardness, with higher values indicating harder materials.[45] Therefore, our values imply that the cubic structure should be harder than the orthorhombic. However, the geometry of the structures has to be taken into account, and thus, the shear modulus (G) is required to make any comment on the relative hardness of the two materials,

$$B^c = \frac{C_{11} + 2C_{12}}{3}, \tag{3}$$

$$B^o = \frac{C_{11} + C_{22} + C_{33} + 2(C_{12} + C_{13} + C_{23})}{9}. \tag{4}$$

2. Shear modulus (G)

G (Eqs. (5) and (6)) is the relation between shear stress and shear strain (i.e., resistance to plastic deformation). G was found to be 137.58 GPa for the cubic and 90.15 GPa for the orthorhombic phase. A large shear modulus is related to a larger resistance against elastic shear strain and surface penetration, which in turn is proportional to hardness.[45] According to our results, cubic $SmCoO_3$ is more resistant to surface penetration than the orthorhombic phase, reinforcing the suggestion that the cubic phase is harder than the orthorhombic one,

$$G^c = \frac{C_{11} - C_{12} + 3C_{44}}{5}, \tag{5}$$

$$G^o = \frac{C_{11} + C_{22} + C_{33} - C_{12} - C_{13} - C_{23}}{15} + \frac{C_{44} + C_{55} + C_{66}}{5}. \tag{6}$$

3. B/G ratio

The B/G ratio gives empirical information on a material's plastic properties. A material with a B/G ratio larger than 1.75 is expected to be ductile, whereas a B/G smaller than 1.75 describes a brittle material. The B/G for $SmCoO_3$ calculated here is found to be 1.49 for the cubic structure and 1.41 for the orthorhombic phase, which puts both polymorphs in the brittle category. No previous reports on $SmCoO_3$'s brittleness have been found, but a study on the related cobaltite perovskite, $LaCoO_3$, showed that it is brittle,[56] thus making it plausible that $SmCoO_3$ should be brittle as well.

4. Poisson ratio (σ)

Poisson's ratio (σ) (Eqs. (7) and (8)) is defined as the ratio of lateral to longitudinal strain in the elastic region while

being under uniform uniaxial stress, and relates to the change in a material during uniaxial stress.[53] It could be used to provide information on interatomic forces. Covalent materials have $\sigma < 0.1$, whereas for ionic materials σ is higher than 0.25.[22] σ for the cubic structure is here calculated to be 0.14, whereas σ for the orthorhombic structure is 0.21, indicating that the latter structure is more ionic than the cubic phase, although each structure has both ionic and covalent character,[57]

$$\sigma^c = \frac{C_{12}}{C_{11} + C_{12}}, \tag{7}$$

$$\sigma^o = \frac{\frac{3B^o}{2} - G^o}{3B^o + G^o}. \tag{8}$$

5. Young's modulus (E)

From B and G, Young's modulus (E), commonly known as the elastic modulus, can be obtained through Eq. (9).[47] E represents the slope of the elastic region in a stress-strain curve. The expression for E is the same for both structures, but their values differ.[47,49] Cubic $SmCoO_3$ was found to have an E of 337.11 GPa, whereas E for the orthorhombic phase was only 218.60 GPa. The smaller E for the orthorhombic system shows that this phase is more receptive to physical changes than its cubic counterpart, which fits with the reasoning above regarding their relative hardnesses,

$$E = \frac{9BG}{3B + G}. \tag{9}$$

6. Elastic anisotropy (A)

Elastic anisotropy (A) is measured for the (100), (010), and (001) shear planes, which in the cubic symmetry (Eq. (10)) are identical, but different in the orthorhombic structure (Eqs. (11)–(13)).[49] This property describes a material's tendency to form micro-cracks.[22] An elastic anisotropy value of 1 indicates an isotropic crystal, whereas deviation indicates shear anisotropy. Here, all $A \neq 1$, indicating that the behavior of the two crystals will be dependent on the stress direction,

$$A^c = \frac{2C_{44}}{C_{11} - C_{12}}, \tag{10}$$

$$A_1^o = \frac{4C_{44}}{C_{22} + C_{33} - 2C_{23}}, \tag{11}$$

$$A_2^o = \frac{4C_{55}}{C_{11} + C_{33} - 2C_{13}}, \tag{12}$$

$$A_3^o = \frac{4C_{66}}{C_{11} + C_{22} - 2C_{12}}. \tag{13}$$

From the elastic constants and calculated mechanical properties, it can then be concluded that the values of the cubic B, G, and E are higher than their orthorhombic counterparts, and that the orthorhombic $SmCoO_3$ is more sensitive to deformation than the cubic phase. These conclusions are in line with the hardness results, which indicate that the cubic polymorph is harder than its orthorhombic counterpart, with a lesser degree of anisotropy. However, comparing the ratio-dependent properties, σ and B/G, we found that both structures exhibit similar brittleness and ductility, which is expected considering that they have the same chemical composition. Consequently, both $SmCoO_3$ phases are prone to fracture, which should be taken into account under SOFC operation.

TABLE V. Mechanical properties of $SmCoO_3$. Bulk modulus (B), shear modulus (G), Young's modulus (E), Poisson's ratio (σ), and anisotropy factor (A) are derived from the elastic constants, which in turn were calculated using DFT+U.

	Cubic	Orthorhombic
B (GPa)	204.46	126.67
G (GPa)	137.58	90.15
B/G	1.49	1.41
E (GPa)	337.11	218.60
σ	0.14	0.21
A^c	0.52	
A_1^o		1.12
A_2^o		1.12
A_3^o		1.51

IV. CONCLUSIONS

In this work, we present a DFT+U study of the magnetic and mechanical properties of the cubic and the orthorhombic $SmCoO_3$ material. We have paid special attention to the magnetic and mechanical properties, which are important when we are considering them as SOFC materials. The electronic ground state for both phases was found to be diamagnetic with the other paramagnetic structures higher in energy. In addition, as also shown experimentally, the orthorhombic phase was lower in energy than the cubic one. In order to introduce the effect of temperature, we mimicked the effect of thermal expansion by increasing the lattice parameter of the bulk material, using the thermal expansion coefficient for orthorhombic $SmCoO_3$. Hence, we were able to determine the coexistence of both the CAFM and the diamagnetic structure in the case of the orthorhombic phase at high temperatures, and a clear stabilization of the CAFM structure for the cubic phase around 1100 K, all in full agreement with the experimental data. These transitions were linked to a large increase in the Co spin state, as well as to a distortion of the unit cell.

Furthermore, we evaluated the most important mechanical properties based on our calculated elastic constants. We found that there were clear differences between the two $SmCoO_3$ polymorphs, relating to anisotropy, bulk, shear, and Young's modulus. It was found that the orthorhombic $SmCoO_3$ exhibits lower hardness than the cubic phase, and that it also has a larger degree of anisotropy. Conversely, both phases exhibited the same ionic/covalent character (σ), and brittleness (B/G). We consider that these results could be helpful in adopting $SmCoO_3$-based perovskites for SOFC use.

ACKNOWLEDGMENTS

The authors acknowledge the Engineering and Physical Sciences Research Council (EPSRC) for financial support (Grant Reference Nos. EP/K016288/1 and EP/K001329/1).

We also acknowledge the use of the UCL Legion High Performance Computing Facility (Legion@UCL) in the completion of this work. Finally, via our membership of the UK's HPC Materials Chemistry Consortium, which is funded by EPSRC (No. EP/L000202), this work made use of the facilities of ARCHER, the UK's national high-performance computing service, which is funded by the Office of Science and Technology through EPSRC's High End Computing Programme. N.H.d.L. thanks the Royal Society for an Industry Fellowship. E.O. gratefully acknowledges EPSRC funding of the Centre for Doctoral Training in Molecular Modelling and Materials Science (No. EP/G036675/1).

[1] B. C. Steele and A. Heinzel, Nature **414**, 345 (2001).
[2] C. Xia, W. Rauch, F. Chen, and M. Liu, Solid State Ionics **149**, 11 (2002).
[3] H.-T. Chen, P. Raghunath, and M. C. Lin, Langmuir **27**, 6787 (2011).
[4] H. Shimada, T. Yamaguchi, T. Suzuki, H. Sumi, K. Hamamoto, and Y. Fujishiro, J. Power Sources **302**, 308 (2016).
[5] K. H. Jung, S. Choi, H.-H. Park, and W.-S. Seo, Curr. Appl. Phys. **11**, S260 (2011).
[6] R. Liu, D. Xu, S. Li, Z. Lü, Y. Xue, D. Wang, and W. Su, Front. Chem. China **1**, 398 (2006).
[7] S. W. Baek, J. H. Kim, and J. Bae, Solid State Ionics **179**, 1570 (2008).
[8] J. H. Kim, S.-W. Baek, C. Lee, K. Park, and J. Bae, Solid State Ionics **179**, 1490 (2008).
[9] H. Fan and M. Han, Faraday Discuss. **182**, 477 (2015).
[10] H. Fukunaga, M. Koyama, N. Takahashi, C. Wen, and K. Yamada, Solid State Ionics **132**, 279 (2000).
[11] I. Fullarton, J. Jacobs, and H. Van Benthem, Ionics **1**, 51 (1995).
[12] X. Jiang, Q. Xu, Y. Shi, X. Li, W. Zhou, H. Xu, and Q. Zhang, Int. J. Hydrogen Energy **39**, 10817 (2014).
[13] Y.-W. Ju, T. Inagaki, S. Ida, and T. Ishihara, J. Electrochem. Soc. **158**, B825 (2011).
[14] S. K. Sahu, S. Tanasescu, B. Scherrer, C. Marinescu, and A. Navrotsky, J. Mater. Chem. A **3**, 19490 (2015).
[15] F. Capon, A. Boileau, C. Carteret, N. Martin, P. Boulet, and J. F. Pierson, J. Appl. Phys. **114**, 113510 (2013).
[16] N. K. Gaur and R. Thakur, Metall. Mater. Trans. A **44**, 5876 (2013).
[17] B. Sathyamoorthy, P. M. Md Gazzali, C. Murugesan, and G. Chandrasekaran, Mater. Res. Bull. **53**, 169 (2014).
[18] M. Tachibana, T. Yoshida, H. Kawaji, T. Atake, and E. Takayama-Muromachi, Phys. Rev. B **77**, 94402 (2008).
[19] T. N. Vasil'chikova, T. G. Kuz'mova, A. A. Kamenev, A. R. Kaul', and A. N. Vasil'ev, JETP Lett. **97**, 34 (2013).
[20] J. Malzbender, R. W. Steinbrech, and L. Singheiser, J. Mater. Res. **18**, 929 (2003).
[21] O. Yamamoto, Electrochim. Acta **45**, 2423 (2000).
[22] A. Roldan, D. Santos-Carballal, and N. H. de Leeuw, J. Chem. Phys. **138**, 204712 (2013).
[23] M. A. Farhanand M. J. Akhtar, J. Phys.: Condens. Matter **22**, 075402 (2010).
[24] G. Kresse and J. Furthmüller, Comput. Mater. Sci. **6**, 15 (1996).
[25] G. Kresse and J. Hafner, Phys. Rev. B **47**, 558 (1993).
[26] G. Kresse and J. Hafner, Phys. Rev. B **49**, 14251 (1994).
[27] G. Kresse and J. Furthmüller, Phys. Rev. B **54**, 11169 (1996).
[28] J. Perdew, K. Burke, and M. Ernzerhof, Phys. Rev. Lett. **77**, 3865 (1996).
[29] J. Perdew, K. Burke, and M. Ernzerhof, Phys. Rev. Lett. **78**, 1396 (1997).
[30] P. E. Blöchl, Phys. Rev. B **50**, 17953 (1994).
[31] P. E. Blöchl, O. Jepsen, and O. K. Andersen, Phys. Rev. B **49**, 16223 (1994).
[32] H. J. Monkhorst and J. D. Pack, Phys. Rev. B **13**, 5188 (1976).
[33] S. Dudarev, G. Botton, and S. Savrasov, Phys. Rev. B **57**, 1505 (1998).
[34] E. Olsson, X. Aparicio-Anglès, and N. H. de Leeuw, J. Chem. Phys. **145**, 14703 (2016).
[35] H. Tu and Y. Takeda, Solid State Ionics **100**, 283 (1997).
[36] A. Wold and R. Ward, J. Am. Chem. Soc. **76**, 1029 (1954).
[37] C. R. Michel, E. Delgado, G. Santillán, A. H. Martínez, and A. Chávez-Chávez, Mater. Res. Bull. **42**, 84 (2007).
[38] M. Alifanti, G. Bueno, V. Parvulescu, V. I. Parvulescu, and V. Cortés Corberán, Catal. Today **143**, 309 (2009).
[39] R. Scurtu, S. Somacescu, J. M. Calderon-Moreno, D. Culita, I. Bulimestru, N. Popa, A. Gulea, and P. Osiceanu, J. Solid State Chem. **210**, 53 (2014).
[40] A. M. Ritzmann, M. Pavone, A. B. Muñoz-García, J. A. Keith, and E. A. Carter, J. Mater. Chem. A **2**, 8060 (2014).
[41] J. Perez-Cacho, J. Blasco, J. Garcia, and R. Sanchez, J. Solid State Chem. **150**, 145 (2000).
[42] Y.-L. Lee, J. Kleis, J. Rossmeisl, and D. Morgan, Phys. Rev. B **80**, 224101 (2009).
[43] P. Ravindran, A. Kjekshus, H. Fjellvåg, A. Delin, and O. Eriksson, Phys. Rev. B **65**, 64445 (2002).
[44] N. Orlovskaya, M. Lugovy, S. Pathak, D. Steinmetz, J. Lloyd, L. Fegely, M. Radovic, E. A. Payzant, E. Lara-curzio, L. F. Allard, and J. Kuebler, J. Power Sources **182**, 230 (2008).
[45] I. R. Shein, V. L. Kozhevnikov, and A. L. Ivanovskii, Solid State Sci. **10**, 217 (2008).
[46] Y. Le Page and P. Saxe, Phys. Rev. B **65**, 1 (2002).
[47] Y. Wu and W. Hu, Eur. Phys. J. B **60**, 75 (2007).
[48] M. Lei, H. Ledbetter, and Y. Xie, J. Appl. Phys. **76**, 2738 (1994).
[49] C. Jiang, S. G. Srinivasan, A. Caro, and S. A. Maloy, J. Appl. Phys. **103**, 43502 (2008).
[50] J. H. Li, Y. Dai, and X. D. Dai, Intermetallics **31**, 292 (2012).
[51] C. R. A. Catlow, M. Dixon, and W. C. Mackrodt, *Computer Simulation of Solids* (Springer-Verlag, Berlin, Heidelberg, 1982).
[52] R. Johnson, Phys. Rev. B **6**, 2094 (1972).
[53] D. Askeland and P. Fulay, *Essentials of Materials Science and Engineering - SI Version*, 2nd ed. (Cengage Learning, 2009).
[54] M. Friák, T. Hickel, B. Grabowski, L. Lymperakis, A. Udyansky, A. Dick, D. Ma, F. Roters, L.-F. Zhu, A. Schlieter, U. Kühn, Z. Ebrahimi, R. A. Lebensohn, D. Holec, J. Eckert, H. Emmerich, D. Raabe, and J. Neugebauer, Eur. Phys. J. Plus **126**, 101 (2011).
[55] J.-S. Zhou, J. B. Goodenough, and J. Yan, Phys. Rev. B **71**, 220103 (2005).
[56] G. Gogotsi, V. Galenko, B. Ozerskii, and N. Orlovskaya, Refract. Ind. Ceram. **42**, 341 (2001).
[57] K. Knížek, Z. Jirák, J. Hejtmánek, M. Veverka, M. Maryško, G. Maris, and T. T. M. Palstra, Eur. Phys. J. B **47**, 213 (2005).